Available online at www.sciencedirect.com

ScienceDirect

Geochimica et Cosmochimica Acta 237 (2018) 223–239

Geochimica et Cosmochimica Acta

www.elsevier.com/locate/gca

Benthic fluxes of metals into the Pearl River Estuary based on $^{224}Ra/^{228}Th$ disequilibrium: From alkaline earth (Ba) to redox sensitive elements (U, Mn, Fe)

Qingquan Hong [a,b], Pinghe Cai [a,b,*], Walter Geibert [c], Zhimian Cao [a,b], Ingrid Stimac [c], Lingfeng Liu [a,b], Qing Li [a,b]

[a] State Key Laboratory of Marine Environmental Science, Xiamen University, Xiamen 361005, PR China
[b] College of Ocean and Earth Sciences, Xiamen University, Xiamen 361005, PR China
[c] Alfred-Wegener Institute, Helmholtz Centre for Polar and Marine Research, Bremerhaven 27570, Germany

Received 26 January 2018; accepted in revised form 28 June 2018; Available online 6 July 2018

Abstract

We extended the $^{224}Ra/^{228}Th$ disequilibrium approach to examine benthic fluxes of a variety of metals, ranging from alkaline earth (Ba) to redox sensitive elements (U, Mn, and Fe), into the Pearl River Estuary (PRE), China. Depth profiles of ^{224}Ra and ^{228}Th in bulk sediment, as well as dissolved ^{224}Ra and trace metals in porewater were measured along a transect within the estuary in July 2015. Significant deficit of ^{224}Ra relative to ^{228}Th was commonly observed in the upper 0–15 cm sediment. We took advantage of the $^{224}Ra/^{228}Th$ disequilibrium in the bottom sediments to construct a full mass balance of ^{224}Ra in the overlying water column. We demonstrated that porewater exchange (PEX) processes with scale lengths of several centimeters are the predominant mechanism for solute transport between sediments and overlying waters in the PRE. In contrast, deep porewater flow or submarine groundwater discharge (SGD) with scale lengths of "meters to kilometers" are a negligible component in the water column budget of ^{224}Ra.

Strong correlations between dissolved ^{224}Ra and trace metals (Ba, U, Mn, and Fe) in porewater were frequently observed in the study region. This likely reflects a fact that geochemical cycling of alkaline earth elements (e.g., Ra and Ba) and redox sensitive elements (like U) in sediments was closely linked to diagenetic reactions of manganese and iron oxides. This linkage makes it possible to quantify benthic fluxes of alkaline earth and redox sensitive metals using $^{224}Ra/^{228}Th$ disequilibrium in sediments. Benthic Ba fluxes based on $^{224}Ra/^{228}Th$ disequilibrium were found to vary from virtually nil to 320 $\mu mol\ m^{-2}\ d^{-1}$ within the PRE. The highest flux was identified at salinity = 3.0–7.8 and could lead to an elevation of 54 $nmol\ Ba\ l^{-1}$ in the water column, which well reproduced the Ba excess frequently observed in the low salinity domain of the estuary. Benthic fluxes of redox sensitive U ranged from −0.42 ("−" denotes flux into sediment) to 1.3 $\mu mol\ m^{-2}\ d^{-1}$. This could only cause a change of −0.1 to 0.3 $nmol\ U\ l^{-1}$ in the water column, which is very small when compared to the U concentration of 13–14 $nmol\ l^{-1}$ in the northern South China Sea. We therefore predicted that water column U in the PRE must behave conservatively during mixing. This prediction is consistent with historical measurements of water column U concentration within the PRE. Large benthic fluxes of Mn and Fe were generally acquired with the $^{224}Ra/^{228}Th$ disequilibrium method. They varied from virtually nil up to 97 $mmol\ m^{-2}\ d^{-1}$, and from zero to 27 $mmol\ m^{-2}\ d^{-1}$, respectively. These estimates are 1–2 orders of magnitude higher than historical measurements based on the traditional incubation method in other coastal settings.

* Corresponding author at: State Key Laboratory of Marine Environmental Science, Xiamen University, Xiamen 361005, PR China.
E-mail address: Caiph@xmu.edu.cn (P. Cai).

https://doi.org/10.1016/j.gca.2018.06.036

Nonetheless, they are in agreement with a simple consideration of Mn and Fe mass balances in the sediment. An important implication of this study is that the role of coastal sediments in estuarine geochemistry of trace metals may need to be re-evaluated.

Keywords: Trace metals; $^{224}Ra/^{228}Th$ disequilibrium; Benthic fluxes; Pearl River Estuary

1. INTRODUCTION

Trace metals play a pivotal role in ocean biogeochemistry. Transition elements Fe and Mn are essential micronutrients for marine phytoplankton (e.g., Martin et al., 1990; Middag et al., 2011), and fluctuations in their supply rates to the open ocean were presumably responsible for the glacial/interglacial cycles in atmospheric carbon dioxide concentration in the geological past (e.g., Martin, 1990). Alkaline earth element Ba generally bears a strong linear relationship with silicate in the oceans (e.g., Chow and Goldberg, 1960). Hence it is considered to be a nutrient-like element and has been extensively used as a proxy of paleoproductivity (e.g., Dymond et al., 1992). In oxygenated seawater, uranium exists as stable uranyl-carbonate complex $UO_2(CO_3)_3^{4-}$ (e.g., Langmuir, 1978). However, when the redox potential is sufficiently low, U(VI) can be reduced into insoluble U(IV) and be removed from the water column. As such, it has been widely used as a paleoredox proxy (e.g., Scholz et al., 2014). Quantitative knowledge of addition and removal processes of these trace metals is critically important for a better understanding of ocean biogeochemistry and for their full utilization as geochemical proxies.

Rivers are a major pathway by which trace metals sourced from continental weathering are transported into the open ocean. However, estuaries connecting rivers and the ocean greatly modify the river-transported signals through a variety of addition and removal processes. For instance, when plotted with respect to salinity, dissolved Ba concentrations fall above the theoretical dilution line in the estuarine mixing zone. These Ba excesses were ascribed either to its desorption from river-borne particles (e.g., Li and Chan, 1979), or to submarine discharge of groundwater with high concentration of Ba (e.g., Moore, 1997). In most estuaries, there is a linear correlation between dissolved U concentration and salinity, indicative of conservative behavior of U during estuarine mixing. However, removal and addition of U from and to the water column have also been documented in some estuaries. Removal of U during estuarine mixing was ascribed to the uptake of this element into bottom sediments under suboxic conditions (e.g., Carroll and Moore, 1993). Likewise, addition of U was interpreted as a result of the input of sediment porewater with elevated U concentration (McKee et al., 1987). Mn and Fe play an extremely important role in estuarine geochemistry because their oxide and hydroxide compounds are effective scavengers for a wide range of trace metals. Under certain estuarine conditions, Mn may behave in a conservative manner (e.g., Holliday and Liss, 1976). However, as a redox-sensitive element, Mn readily undergoes redox transformation between Mn (II) and Mn(IV). During estuarine mixing, a large portion of soluble Mn(II) delivered by rivers can be oxidized into insoluble Mn(IV) oxides and subsequently be removed from the water column. Conversely, the reduction of Mn (IV) oxides in anoxic estuarine sediments during early diagenesis releases Mn(II) into the ambient porewater, which may subsequently migrate upward into the overlying water column. As a consequence, Mn exhibits various behaviors in different estuaries (e.g., Knox et al., 1981; Joung and Shiller, 2016). In contrast to Mn, removal of dissolved Fe has been commonly observed during estuarine mixing, and was ascribed to the salt-induced flocculation and precipitation of Fe-humic colloids (e.g., Boyle et al., 1977). Nonetheless, due to the diagenetic reduction of Fe(III) oxides, porewaters in anoxic estuarine sediments are typically enriched in dissolved Fe(II), the concentration of which can be several orders of magnitude higher than that of the overlying water. As such, if some fraction of Fe(II) in porewater escapes into the overlying water column, it could exert an impact on the estuarine geochemistry of Fe.

Overall, evidence for the important role of bottom sediments in estuarine geochemistry of trace metals is not in dispute. However, it is a major challenge in marine chemistry to accurately quantify benthic fluxes of trace metals, particularly in very dynamic estuarine settings. Historical measurements of benthic trace metal fluxes might be biased due to the inherent limitations associated with the traditional core incubation method (e.g., Shi et al., 2018). In this aspect, the recently developed $^{224}Ra/^{228}Th$ disequilibrium approach circumvents the difficulty of imposing interference on the natural system with the incubation method, and has been proven to be a robust tool for quantifying benthic fluxes of dissolved inorganic carbon (DIC) and nutrients from coastal sediments (e.g., Cai et al., 2014, 2015; Hong et al., 2017). Here, we extend this approach to examine benthic fluxes of trace metals (i.e., Ba, U, Mn, and Fe) into the Pearl River Estuary (PRE), China. Our results will provide a new perspective on estuarine geochemistry of trace metals.

2. SAMPLING AND ANALYTICAL METHODS

2.1. Study area

The PRE, a north-south bell-shaped estuary with an area of ~1180 km^2, is located in the southern China (Fig. 1). It receives ~55% of the freshwater and ~46% of the particles discharged by the Pearl River (Zhao, 1990). As a result, the estuary is characterized by high sedimentation rates of >1.0–7.0 cm yr^{-1} (Chen, 1991; Zhou et al., 2004). Fine-grained sediments cover >90% of the seabed within the estuary. In summer, the benthos is dominated

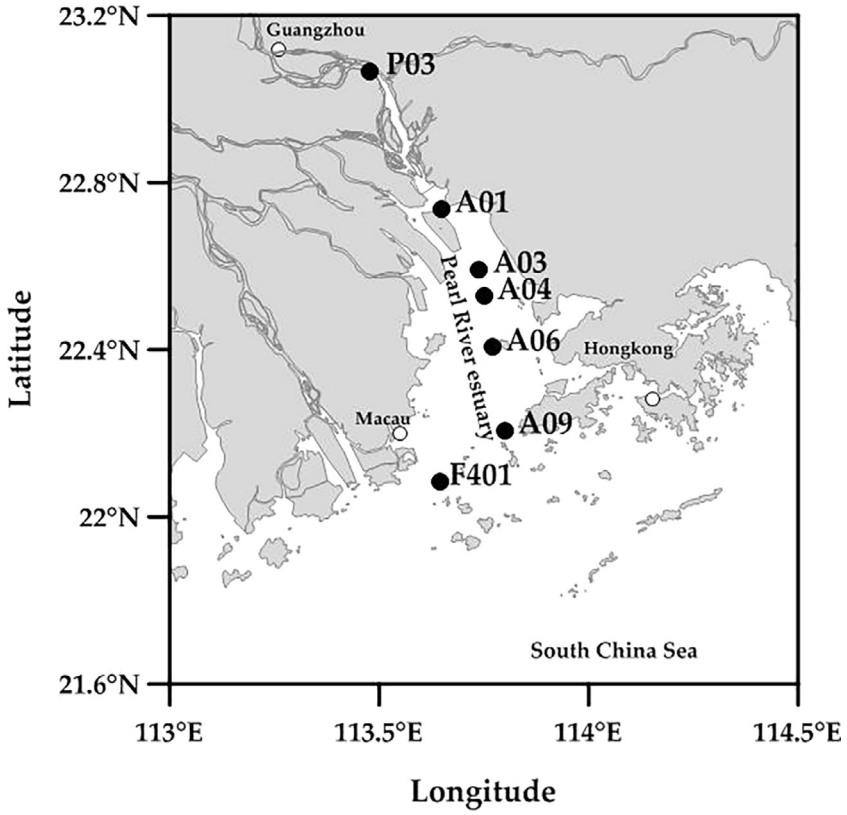

Fig. 1. Sampling locations in the Pearl River Estuary in July 2015.

by polychaetes and crustacea, and the biomass increases with salinity and water depth (Zhang, 2014).

Sediment and seawater samples were collected along a transect within the PRE in July 2015 (Fig. 1). Intact sediment cores were collected using a standard box corer. Overlying water in the box corer was sampled to characterize the extent of $^{224}Ra/^{228}Th$ disequilibrium on suspended particles. Sediment sub-cores were retrieved by carefully inserting PVC tubes with an inner diameter (i.d.) of 47 or 65 mm into the bulk sediment. Sediment subcores (i.d. = 47 mm) were sliced into 1-cm thick slabs and were used for the analyses of ^{224}Ra, ^{228}Th, and porosity in bulk sediment. Porewater samples were extracted from several parallel sediment subcores (i.d. = 65 mm) using Rhizon samplers. Prior to the cruise, the Rhizon samplers were soaked in sub-boiled 2 mol l^{-1} HNO_3, washed with Milli-Q water and dried in a laminar flow hood set in a clean lab. Porewater samples for trace metal analyses were acidified (2 µl of double-distilled concentrated HCl (Merck) per ml porewater) and transferred into 10 ml LDPE tubes. In parallel to sediment sampling, water samples for the analyses of ^{224}Ra were also collected using Niskin bottles mounted on a CTD rosette system.

2.2. Analytical methods

2.2.1. ^{224}Ra and ^{228}Th

The analytical method for ^{224}Ra and ^{228}Th in sediments and suspended particles has been detailed in Cai et al. (2012). Briefly, to the 1-cm thick sediment slabs Milli-Q water was added and the sample was sonicated to generate a slurry. After adjustment of the pH, $KMnO_4$ and $MnCl_2$ solutions were added to form a suspension of MnO_2. The slurry together with the MnO_2 suspension was filtered evenly onto a 142 mm GFF filter. Subsequently, the sample was counted on a RaDeCC system for 4–6 h. After 8–10 days and ~25 days, the sample was re-counted in the same RaDeCC system. ^{224}Ra and ^{228}Th activities in bulk sediment can be calculated either from the first and second measurements, or from the first and third measurements.

Porewater ^{224}Ra was co-precipitated by adding $KMnO_4$ and $MnCl_2$ solutions to the samples. The resultant MnO_2 precipitate was filtered onto a 142 mm GFF filter and counted on a RaDeCC system for 10 h. Seawater ^{224}Ra was quantitatively pre-concentrated onto a column of MnO_2-impregnated fiber and measured on a RaDeCC system according to the classic procedure presented by Moore and Arnold (1996). Detection efficiency of the counter was calibrated with a ^{232}U-^{228}Th standard prepared in the same manner as the samples.

2.2.2. Trace metals (Ba, U, Mn, and Fe)

Porewater samples were diluted 30–100 fold with a 1.0 M double-distilled HNO_3 solution. A succession of external calibration standards were prepared from certified stock solutions, and were used to calculate the results. Analyses were performed using an Element II ICP-MS in Alfred-Wegener Institute for Polar and Marine Research,

Germany. A known quantity of ^{103}Rh was added as the internal standard to monitor the instrument statue over the sample run. Ba and U were measured in low resolution mode, whereas Fe and Mn in medium resolution mode. A standard solution prepared by digesting certified Standard Reference Material (SRM 2702) was used to assess the accuracy of our measurements. Overall, the analytical errors (RSD) were better than 5%. The detection limits of Ba, U, Mn, and Fe were 3.0, 0.01, 17, and 61 nmol l^{-1}, respectively. The procedural blank for sampling and analyses were lower than the detection limits.

2.2.3. Sediment porosity

Total suspended matter (TSM) was determined by filtering a certain volume of seawater onto a pre-weighted Nuclepore filter. The sample was dried at 60 °C to a constant weight. TSM was calculated as the weight difference of the dry sample and the filter. As with TSM, wet sediment samples were dried at 60 °C. Porosities were calculated from the weight loss using a solid density of 2.6 g cm^{-3} and corrected for the salt content.

3. RESULTS

^{224}Ra and ^{228}Th data for bulk sediment and suspended particles, as well as porewater data of ^{224}Ra and trace metals are compiled in Appendix A. Also presented are sediment porosity and dissolved oxygen content in bottom water. ^{224}Ra activities, temperature, salinity, and total suspended matter content (TSM) in the water column are listed in Appendix B.

3.1. Quality of ^{224}Ra and ^{228}Th measurements

Errors associated with ^{224}Ra and ^{228}Th activities are propagated from counting statistic, counter calibration, chance coincidence correction, and decay/ingrowth correction. For the ^{224}Ra/^{228}Th disequilibrium approach, it is vitally important to have a precise and accurate determination of ^{224}Ra and ^{228}Th in bulk sediment, particularly in areas where the disequilibrium, i.e., difference between total ^{224}Ra and ^{228}Th, is expected to be small. We do this by: (1) performing the measurements on RaDeCC counters within <12 h after sample collection to lower the uncertainty induced by decay/ingrowth correction; (2) counting ^{224}Ra and ^{228}Th activities to a statistic error that is generally <2%; (3) using the standard addition method (e.g., Cai et al., 2012) to achieve an accuracy of ~1–2% for counter calibration (Fig. 2a). The propagated error on ^{224}Ra and ^{228}Th activities in bulk sediment averages ±3–4% for the entire data set (Appendix A), compared to an overall accuracy of ±5–7% at the developing stage of this method (e.g., Cai et al., 2012). We have verified the performance of our method by comparing the replicate measurements of ^{228}Th in the same samples, i.e., ^{228}Th activities calculated from the first and second measurements (^{228}Th$_{1,2}$), and from the first and third measurements (^{228}Th$_{1,3}$). We found a mean ^{228}Th$_{1,3}$/^{228}Th$_{1,2}$ ratio of 1.013 ± 0.048 (1 SD, n = 77). Note that the standard deviation is consistent with the error propagated from the uncertainty of two replicate measurements. It should also be mentioned that the final ^{228}Th activities are the averages of ^{228}Th$_{1,2}$ and ^{228}Th$_{1,3}$.

We have further confirmed the performance of our method through ^{228}Th measurements in replicate sediment cores. Three sediment cores were collected separately from a same location at a tidal flat in the German Wadden Sea (53.8476°N, 8.5734°E) over a 12-day period in September 2017. Activities of ^{228}Th in bulk sediment were determined using the protocol described above in Alfred-Wegener Institute for Polar and Marine Research, Germany. As shown in Table 1 and Fig. 2b, measurements of ^{228}Th for replicate samples are highly consistent at any specific

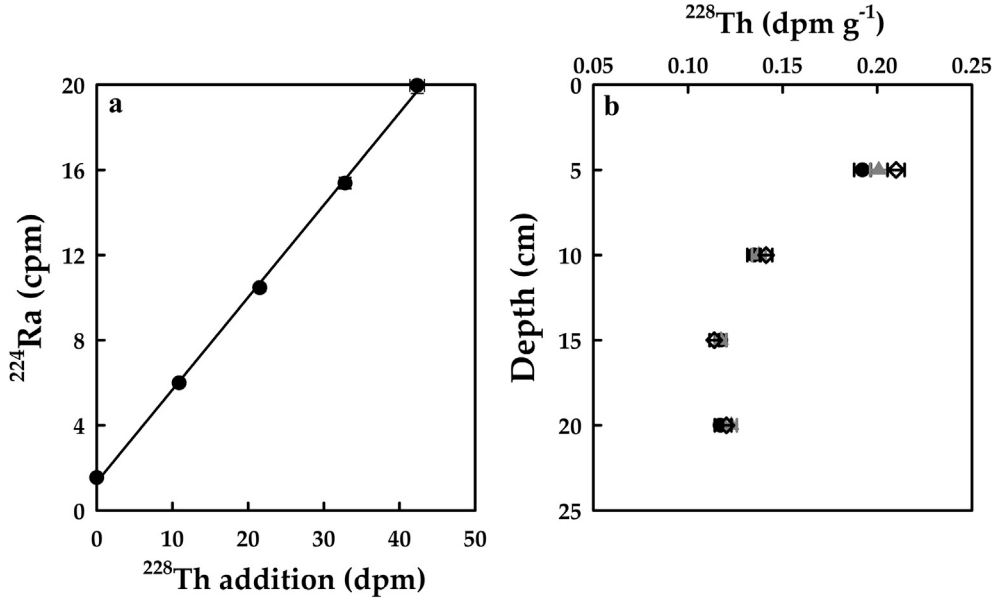

Fig. 2. (a) Calibration of the RaDeCC system using the method of standard addition. The slope of the regression is 0.434 and the associated uncertainty is 0.0077, i.e., <2%. (b) Comparison of ^{228}Th measurements in replicate sediment cores collected from a tidal flat in the German Wadden Sea. The black circles, gray triangles and open diamonds denote the measurements of replicate core R1, R2 and R3, respectively.

Table 1
Measurement of ^{228}Th activities in three replicate sediment cores (R1, R2, and R3) collected from a tidal flat (53.8476°N, 8.5734°E) in the German Wadden Sea.

Depth (cm)	^{228}Th-R1 (dpm g^{-1})	^{228}Th-R2 (dpm g^{-1})	^{228}Th-R3 (dpm g^{-1})	Average ^{228}Th ± SD (dpm g^{-1})
4–5	0.192 ± 0.005	0.201 ± 0.005	0.210 ± 0.005	0.201 ± 0.009
9–10	0.135 ± 0.004	0.137 ± 0.004	0.141 ± 0.003	0.138 ± 0.003
14–15	0.117 ± 0.003	0.117 ± 0.003	0.114 ± 0.002	0.116 ± 0.002
19–20	0.117 ± 0.003	0.123 ± 0.003	0.120 ± 0.003	0.120 ± 0.003

depth. The standard deviation of replicate measurements (RSD) falls in the range of <2–5%. While the standard deviation may also include some real variations caused by heterogeneity of the sediment, it is consistent with the uncertainty (±3–4%) associated with an individual measurement of ^{228}Th. This strongly suggests that the uncertainties reported here are a real reflection of the overall accuracy/precision of ^{224}Ra/^{228}Th disequilibrium measurements in the sediment.

3.2. Distribution of ^{228}Th and ^{224}Ra

3.2.1. Vertical profiles of ^{228}Th and ^{224}Ra in the sediment

Vertical profiles of ^{228}Th and total ^{224}Ra in the near-surface sediments are shown in Fig. 3. During the survey in July 2015, ^{228}Th activities varied from 1.17 ± 0.03 to 6.64 ± 0.18 dpm g^{-1}, significantly higher than our prior measurements (0.97 ± 0.03–3.34 ± 0.08 dpm g^{-1}) in November 2013 (independent *t*-test, $P < 0.001$) (Cai et al., 2015). The most prominent difference was observed at the river mouth (St. P03), where sediment ^{228}Th activities obtained in July 2015 (4.06 ± 0.09–6.64 ± 0.18 dpm g^{-1}) were a factor of two higher than those in November 2013 (1.61 ± 0.06–2.99 ± 0.11 dpm g^{-1}). This change was in pace with the seasonal trends of the input of terrestrial particulate matter into the PRE, which peaks between May and July, but lowers in the dry season (November–March) (Ni et al., 2008). ^{228}Th is produced from the decay of its lithogenic progenitor ^{232}Th. As such, changes in the ^{228}Th activities may reflect an alteration of the sediment mineralogy, which in turn could be caused by the seasonal variations in the terrestrial input into the PRE. Nonetheless, depth profiles of ^{228}Th collected in July 2015 and in November 2013 shared some common features. They generally showed a minimum at a depth of 3–5 cm, and relatively constant activities of ^{228}Th below that depth layer (Fig. 3).

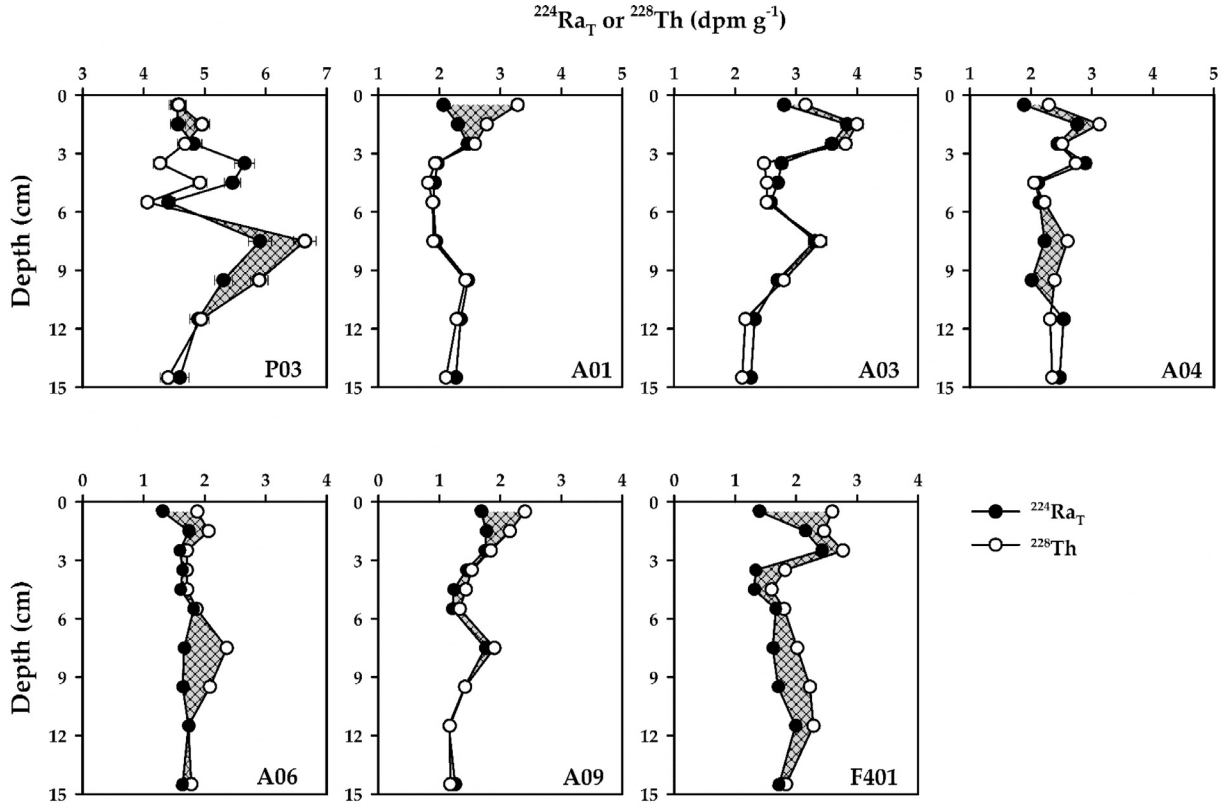

Fig. 3. Vertical profiles of total ^{224}Ra (^{224}Ra$_T$) and ^{228}Th in bulk sediment. Error bars are shown if larger than the symbol size, but on this scale, they are insignificant. The shadowed diagonal area denotes a deficit of ^{224}Ra$_T$ relative to ^{228}Th.

Total ^{224}Ra activities fell in the range of 1.15 ± 0.04–5.91 ± 0.19 dpm g^{-1} during July 2015, significantly higher than those acquired in November 2013 (0.75 ± 0.03–3.20 ± 0.11 dpm g^{-1}). As with our prior study, pronounced deficit of ^{224}Ra relative to ^{228}Th was evident in the upper sediment column at most of the stations (Fig. 3), indicating intense migration of ^{224}Ra out of the sediment. However, compared to our prior study, the loci of the most marked deficit of sediment ^{224}Ra seemed to extend seaward, and were identified at the mid- and outer estuary in July 2015. Notably, at the river mouth (St. P03), both deficit and excess of ^{224}Ra relative to ^{228}Th were observed (Fig. 3). This suggests intense internal migration of ^{224}Ra within the upper sediment column. It is also worthwhile to note that although ^{224}Ra deficit was commonly observed in the study region, it was confined within the upper 0–15 cm sediment. This indicates that solute exchange between the sediment and the overlying water was dominated by processes with scale lengths of centimeters, namely the porewater exchange (PEX) processes (e.g., Hong et al., 2017).

Porewater ^{224}Ra activities ($^{224}Ra_D$) varied from 2.7 ± 1.2 dpm l^{-1} to 54 ± 2.9 dpm l^{-1} during July 2015 (Appendix A), comparable to those obtained in November 2013 (1.1 ± 1.4–56 ± 5.0 dpm l^{-1}). Similar to our previous observations, they were ~1–3 orders of magnitude higher than ^{224}Ra activities in the overlying water (Appendix B), but accounted for <5% of the total ^{224}Ra activity in bulk sediment. $^{224}Ra_D$ generally showed a maximum at depths of ~2–5 cm, and remained relatively constant below this depth.

3.2.2. ^{228}Th and ^{224}Ra in the water column

Similar to previous observations (e.g., Cai et al., 2015; Hong et al., 2017), ^{224}Ra/^{228}Th ratio in suspended particles was >1 at the river mouth (Appendix A), but decreased to an average of 0.43 ± 0.14 (1SD, n = 6) in the mixing zone of the estuary, indicating that ~57% of the exchangeable ^{224}Ra in particulate phase was released during estuarine mixing. Seawater ^{224}Ra activities increased from 19.5 ± 1.3 dpm 100 l^{-1} at the river mouth to a wide plateau of ~50–60 dpm 100 l^{-1} at the mid- and outer estuary (Fig. 4), in stark contrast to a sharp peak of ~100 dpm 100 l^{-1} in the mid estuary that was identified in November 2013 (Cai et al., 2015). This may reflect more intense horizontal estuarine mixing in the wet season (July 2015) as compared to the dry season (November 2013). Alternatively, it could be a result of the seaward extension of the large deficit of sediment ^{224}Ra (and hence high benthic flux of ^{224}Ra) in the wet season.

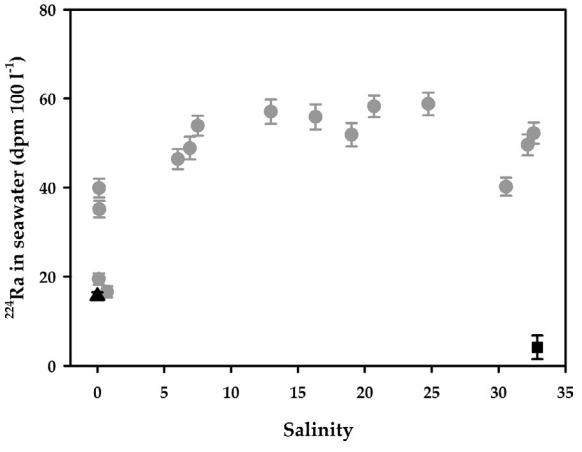

Fig. 4. Distribution of seawater ^{224}Ra activities (gray circle) along a salinity gradient within the Pearl River Estuary. The median value at S = 0 was adopted as the riverine end-member (filled triangle), and the oceanic end-member (filled square) was taken from Wang (2014).

3.3. Distribution of trace metals in porewater

Concentrations of trace metals (Ba, U, Mn, and Fe) in porewater are compiled in Appendix A. Typical depth profiles of these trace metals are compared with porewater profiles of ^{224}Ra in Fig. 5.

3.3.1. Barium

Concentrations of Ba varied between 170 and 3670 nmol l^{-1} (Appendix A). Horizontally, it exhibited a decreasing trend downstream off the river mouth. At the river mouth (P03) and the outermost site (F401), porewater concentration of Ba increased steadily with depth. For the other sites, it generally displayed a maximum at depths of 3–6 cm, and then decreased to a relatively constant level below this depth. As shown in Fig. 5, porewater profiles of Ba generally resembled those of ^{224}Ra. We have even identified a linear relationship of Ba and ^{224}Ra at several locations, like St. P03 and A06. This probably suggests similar geochemical behaviors of Ra and Ba in anoxic estuarine sediments. In addition, concentrations of Ba were found to correlate well with Mn and Fe in porewater (Fig. 6). In estuarine sediments, Ba and ^{224}Ra are mainly absorbed onto Mn(IV) and Fe(III) oxides (Murray, 1975). When Mn(IV) and Fe(III) oxides are reduced into soluble Mn (II) and Fe(II) in the early diagenetic reactions, Ba and ^{224}Ra may be released into the ambient porewater at roughly similar rates, causing a possible correlation of ^{224}Ra, Ba, Mn, and Fe in porewater.

3.3.2. Uranium

Porewater concentrations of U varied between 0.78 and 55.8 nmol l^{-1} (Appendix A). Depth profiles of U generally displayed a maximum in the topmost layer (Fig. 5), which was likely caused by the desorption of U from ferric oxides in high-alkalinity conditions (McKee et al., 1987). Below this layer, it either decreased steadily with depth, or exhibited a minimum at depths of 3–6 cm. Notably, the U minima corresponded roughly to the maxima of Fe and Mn in porewater. This depth pattern is a clear display of U geochemistry in marine sediments: in porewater, uranium generally occurs as soluble U(VI); however, when the redox potential is sufficiently low, U(VI) will be reduced into insoluble U(IV) and be removed from porewater. The reduction of U(VI) takes place thermodynamically between Mn(IV) and Fe(III) (Cochran et al., 1986). Furthermore, it has been demonstrated that this reaction can be accelerated

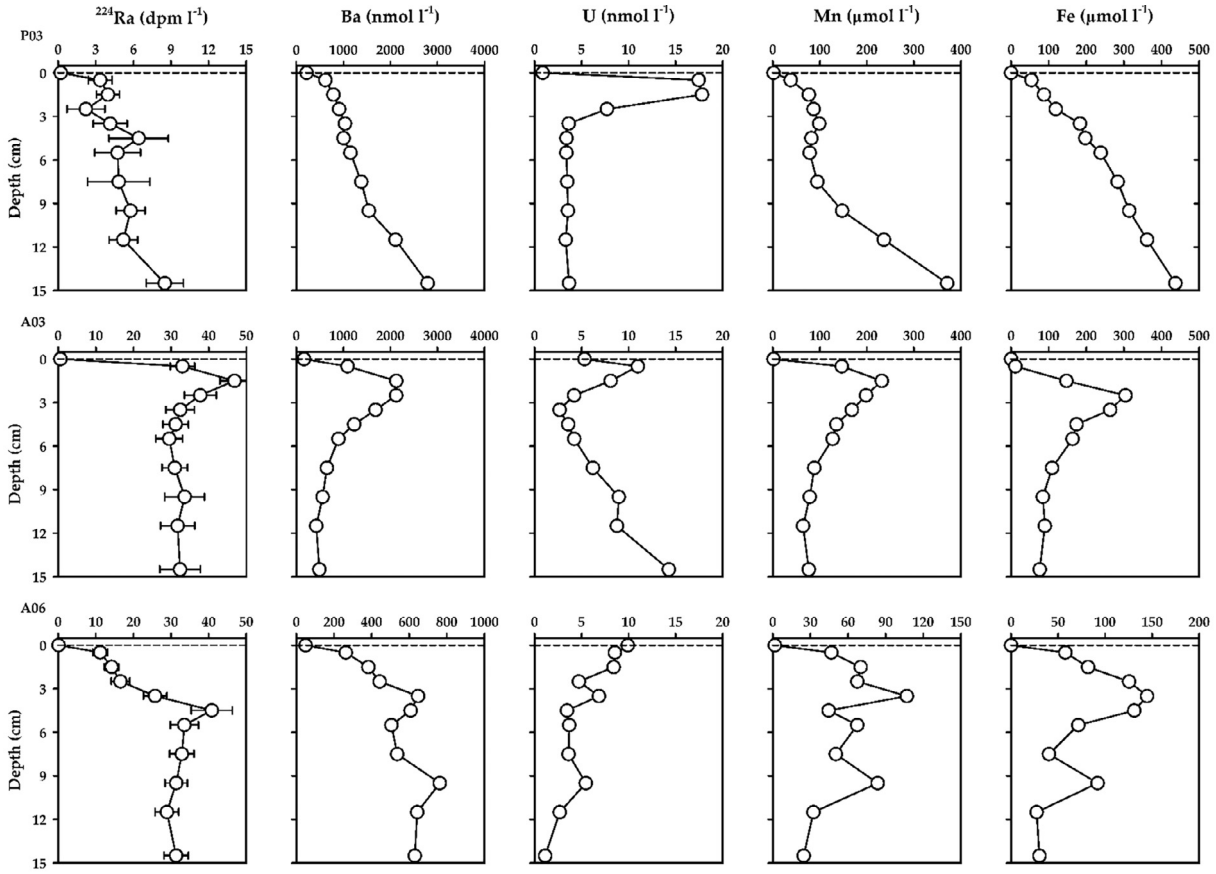

Fig. 5. Typical porewater profiles of ^{224}Ra and trace metals in the near-surface sediments of the Pearl River Estuary. The dash line denotes the sediment–water interface; symbols above the dash line represent measurements in the bottom water.

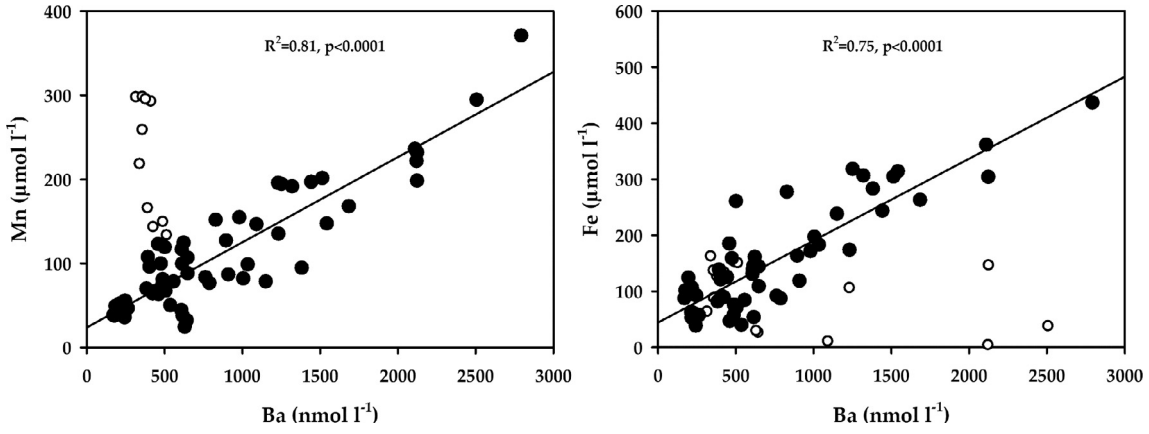

Fig. 6. Correlation of dissolved Mn and Fe vs. Ba in sediment porewater within the Pearl River Estuary. The data in St. F401 (open circle) is not included in the regression as this station is located outside the estuary.

by Fe-reducing microorganisms in sediments (Lovley et al., 1991). Consequently, when Mn(IV) and Fe(III) oxides are reduced into soluble Mn(II) and Fe(II), ^{224}Ra might be released into the ambient porewater. In the meantime, U (VI) will be reduced into insoluble U(IV) and be removed from porewater, thereby leading to a negative correlation between ^{224}Ra and U in porewater as identified at St. A06 ($R^2 = 0.68$, $p < 0.05$).

3.3.3. Manganese and iron

Porewater concentrations of Mn and Fe ranged from 25 to 371 μmol l^{-1}, and from 5.0 to 437 μmol l^{-1}, respectively.

The lowest concentrations of Mn and Fe were generally observed in the topmost sediment layer (Fig. 5). This was likely caused by the re-oxidation of Mn(II) and Fe(II) as they migrate upward to the sediment–water interface. At the river mouth (P03), both Mn and Fe concentrations increased steadily with depth. For the other sampling sites, they commonly exhibited a maximum at depths of 1–6 cm (Fig. 5). Notably, the depth of Mn maximum was generally shallower than that of Fe (Fig. 5 and Appendix A). This phenomenon is a typical manifestation of the free energy-competition hypothesis (Froelich et al., 1979), which predicts preferential utilization of MnO_2 over Fe(III) oxides by organic matter decomposition in marine sediments. The attenuation of Mn and Fe concentrations below these peaks was possibly caused by the precipitation of $MnCO_3$ and FeS, though H_2S was not detectable (detection limit: 2 μM) in the sediment porewater within the PRE.

4. DISCUSSION

4.1. ^{224}Ra budget in the water column

4.1.1. PEX fluxes of ^{224}Ra

Benthic fluxes of ^{224}Ra induced by small scale porewater exchange (PEX) processes were estimated with a one-dimensional steady-state mass balance model as described in Cai et al. (2012):

$$F_{Ra} = \lambda_{Ra} \int_0^z (A_{Th} - A_{Ra}) dz \quad (1)$$

where F_{Ra} represents PEX flux of ^{224}Ra ("+" upward), λ_{Ra} is the decay constant of ^{224}Ra (0.189 d^{-1}), z is the depth horizon where ^{224}Ra and ^{228}Th approach secular equilibrium, A_{Th} and A_{Ra} denote ^{228}Th and ^{224}Ra activities in bulk sediment (unit: dpm cm^{-3}), respectively. PEX fluxes of ^{224}Ra varied from -0.008 ± 0.067 to 0.910 ± 0.053 dpm cm^{-2} d^{-1} in July 2015 (Table 2), and were comparable to a flux range of 0.125 ± 0.070 to 0.656 ± 0.063 dpm cm^{-2} d^{-1} acquired in November 2013 (Cai et al., 2015). Low fluxes of ^{224}Ra were generally observed in the inner estuary, whereas in the mid- and outer estuary, high fluxes of ^{224}Ra were commonly identified (Table 2). This pattern is in line with the distribution mode of ^{224}Ra in the overlying water column (Fig. 4), suggesting porewater exchange as the predominant mechanism for solute transport from the seabed into the PRE.

PEX fluxes of ^{224}Ra are regulated by a variety of exchange processes operating at the sediment–water interface. In cohesive muddy sediments (like the seabed of the PRE), these processes include molecular diffusion, sediment mixing, and irrigation (e.g., Berner, 1980). The relative importance of these processes can be assessed by comparing the theoretical fluxes of ^{224}Ra induced by molecular diffusion (F_M) and sediment mixing (F_B) with the ^{224}Ra fluxes estimated from ^{224}Ra/^{228}Th disequilibrium in sediments (e.g., Cai et al., 2015):

$$F_M = \phi D_S^{Ra} \frac{\partial Ra_D}{\partial z},$$
$$F_B = D_B \frac{\partial(\phi Ra_D)}{\partial z} + D_B \frac{\partial[\rho_S(1-\phi)Ra_S]}{\partial z} \text{ and}$$
$$F_g = F_{Ra} - F_M - F_B \quad (2)$$

where ϕ represents sediment porosity, D_S^{Ra} is the diffusion coefficient of ^{224}Ra in sediments, D_B denotes the sediment mixing rate, F_g is the ^{224}Ra flux induced by irrigation. The concentration gradients $\frac{\partial Ra_D}{\partial z}$ and $\frac{\partial[\rho_S(1-\phi)Ra_S]}{\partial z}$ at the sediment–water interface, i.e., $z = 0$, were computed from ^{224}Ra measurements in the bottom water and the topmost 0–1 cm sediment. Our calculations showed that irrigation, on average, accounted for >90% of the total fluxes of ^{224}Ra (Table 2). This result is consistent with our previous estimates in the Yangtze River Estuary and the Jiulong River Estuary (Cai et al., 2014; Hong et al., 2017).

4.1.2. ^{224}Ra mass balance in the water column

We utilized the benthic fluxes of ^{224}Ra derived from ^{224}Ra/^{228}Th disequilibrium in the bottom sediments to construct a full mass balance of ^{224}Ra in the overlying water column. Supply terms of ^{224}Ra are riverine discharge (F_{Riv}), desorption from suspended particles (F_{Des}), release via porewater exchange (F_{PEX}), and input from deep porewater flow or submarine groundwater discharge (F_{SGD}). Loss of ^{224}Ra occurs principally via radioactive decay (F_{Decay}) and net export to the adjacent sea (F_{E-O}). Consequently, we have:

$$F_{Riv} + F_{Des} + F_{PEX} + F_{SGD} = F_{Decay} + F_{E-O} \quad (3)$$

Table 2
Molecular diffusion coefficient of ^{224}Ra in sediments (D_S^{Ra}), estimated flux ("+": outward) of ^{224}Ra (F_{Ra}) and flux induced by molecular diffusion (F_M), sediment mixing (F_B) and irrigation (F_g) in the sediment within the Pearl River Estuary.

Station	D_S^{Ra} cm^2 d^{-1}	F_{Ra} dpm cm^{-2} d^{-1}	F_M dpm cm^{-2} d^{-1}	[a]F_B dpm cm^{-2} d^{-1}	[b]F_g dpm cm^{-2} d^{-1}
P03	0.466	0.054 ± 0.111	0.003 ± 0.001	0.021 ± 0.003	0.031 ± 0.111
A01	0.480	0.201 ± 0.054	0.008 ± 0.001	0.008 ± 0.001	0.185 ± 0.054
A03	0.448	-0.008 ± 0.067	0.020 ± 0.002	0.021 ± 0.002	-0.050 ± 0.067
A04	0.476	0.239 ± 0.058	0.019 ± 0.002	0.020 ± 0.001	0.200 ± 0.058
A06	0.383	0.781 ± 0.051	0.006 ± 0.001	0.014 ± 0.001	0.760 ± 0.051
A09	0.410	0.358 ± 0.043	0.022 ± 0.002	0.016 ± 0.001	0.320 ± 0.043
F401	0.441	0.910 ± 0.053	0.014 ± 0.002	0.011 ± 0.001	0.886 ± 0.053

[a] An average of the sediment mixing coefficients reported by Cai et al. (2015) was used to estimated F_B.
[b] $F_g = F_{Ra} - F_M - F_B$.

Table 3
Notations used in the text and ^{224}Ra mass balance in the water column of the Pearl River Estuary.

Notation	Description	July 2015		November 2013	
		Value	Error	Value	Error
λ_{Ra} (d^{-1})	Decay constant of ^{224}Ra	0.189		0.189	
V_E (10^{10} m^3)	Water volume of the estuary	1.72		1.63[a]	
C_{TSM} (g m^{-3})	Average concentration of total suspended matter	17.5	2.0	44.6[a]	4.8
[b]Q_{Riv} (m^3 s^{-1})	Total freshwater discharge rate by the Pearl River	11,800	960	8550	4480
[c]τ (d)	Water residence time in the estuary	2.2	0.2	3.0	0.7
A_{228Th} (dpm m^{-3})	Volume-weighted average activity of ^{228}Th on suspended particles	1.81	0.29	2.50[a]	1.13
A_{Riv} (dpm m^{-3})	Activity of dissolved ^{224}Ra in the river end-member	352	19	300[a]	20
A_E (dpm m^{-3})	Volume-weighted average activity of dissolved ^{224}Ra in the estuary	524	73	546[a]	49
A_O (dpm m^{-3})	Activity of dissolved ^{224}Ra in the adjacent sea	41.3	26.4	41.3	26.4
Supply terms					
F_{Riv} (10^{11} dpm d^{-1})	Input of ^{224}Ra via river discharge	1.9	0.19	1.2	0.62
F_{Des} (10^{11} dpm d^{-1})	Supply of ^{224}Ra via desorption	0.56	0.02	1.2[a]	0.06
F_{PEX} (10^{11} dpm d^{-1})	Input of ^{224}Ra via porewater exchange	47.7	12.1	47.0[a]	3.3
F_{SGD} (10^{11} dpm d^{-1})	Input of ^{224}Ra via submarine groundwater discharge	4.5	12.8	−5.0[a]	7.5
Loss terms					
F_{Decay} (10^{11} dpm d^{-1})	Loss of ^{224}Ra via radioactive decay	17.0	2.4	16.9[a]	1.5
F_{E-O} (10^{11} dpm d^{-1})	Loss of ^{224}Ra via net export to the adjacent sea	37.6	3.4	27.5[a]	6.5

V_E was calculated using$V_E = \sum(S_i H_i)$, where S_i denotes the area of the Pearl River Estuary, H_i is the water depth, A_{228Th} was calculated using $A_{228_{Th}} = \frac{\sum(A_{228_{Th,i}} S_i H_i)}{\sum(S_i H_i)}$, A_{Riv} was estimated as the median of ^{224}Ra activities at S = 0, A_E was estimated using $A_E = \frac{\sum(A_i S_i H_i)}{\sum(S_i H_i)}$, where A_i represents the seawater activities of ^{224}Ra, A_O was the average activity of seawater ^{224}Ra at S = 32.9 (Wang, 2014), F_{Riv} was calculated using $F_{Riv} = 0.53 \times A_{Riv} \cdot Q_{Riv}$, where 0.53 denotes the fraction of the total fresh water discharge caught by the Pearl River Estuary, F_{Des} was calculated using $F_{Des} = \lambda_{Ra} \cdot V_E \cdot A_{228_{Th}} \cdot C_{TSM} \cdot f_{Des}$, where f_{Des} denotes the fraction of the exchangeable ^{224}Ra that was released during estuarine mixing (~57%, see Section 3.2.2), F_{PEX} was calculated using $F_{PEX} = \sum F_{Ra,i} \cdot S_i$, F_{Decay} was computed using$F_{Decay} = \lambda_{Ra} \sum A_i \cdot S_i \cdot H_i$, F_{E-O} was calculated using $F_{E-O} = \frac{V_E(A_E - A_O)}{\tau}$. For details, see Cai et al. (2015).

[a] Value calculated using the data set reported in Cai et al. (2015).

[b] Flow rates during the sampling period were recorded hourly at the hydrological stations and downloaded from http://xxfb.hydroinfo.gov.cn/ssIndex.html?type=2.

[c] Values taken from Wang (2014). In November 2013, a transition season in this region, a mean value (3.0 ± 0.7 d) of the wet season and the dry season was used.

Supply and loss terms in the above equation were computed in a way similar to that described in Hong et al. (2017). For comparison, we also constructed ^{224}Ra mass balance in the water column for November 2013 using the ^{224}Ra data set reported in Cai et al. (2015). As shown in Table 3, river input of ^{224}Ra and desorption of ^{224}Ra from suspended particles were 1.9×10^{11} and 0.6×10^{11} dpm d^{-1} for July 2015, and 1.2×10^{11} and 1.2×10^{11} dpm d^{-1} for November 2013, respectively. These source terms accounted for <5% of the total input of ^{224}Ra, and were minor components in the overall budget of ^{224}Ra in the PRE. In comparison, total PEX fluxes of ^{224}Ra were remarkably higher, and show little seasonal variation ($47.7 \pm 12.1 \times 10^{11}$ dpm d^{-1} in July 2015 vs. $47.0 \pm 3.3 \times 10^{11}$ dpm d^{-1} in November 2013). Total SGD fluxes of ^{224}Ra were calculated from Eq. (3) as the difference between the total loss of ^{224}Ra and the sum of the supply terms F_{Riv}, F_{Des}, and F_{PEX}. In this manner, we derived an estimate of $4.5 \pm 12.8 \times 10^{11}$ and $-5.0 \pm 7.5 \times 10^{11}$ dpm d^{-1} for total SGD flux of ^{224}Ra in July 2015 and November 2013, respectively. These estimates are dramatically lower than the total PEX fluxes of ^{224}Ra. In particular, when taking into account the large related uncertainties, they are essentially indiscernible from zero. While both PEX and SGD deliver solutes from the seabed, they represent two different mechanisms for solute transport between sediments and overlying waters. SGD is an advective transport mechanism with scale lengths of meters to kilometers (Moore, 2010). It does not include processes with scale lengths of "millimeters to meters", like molecular diffusion, flow- and topography-induced advection, wave pumping, ripple migration, shear flow, as well as shallow bio-turbation and bio-irrigation (e.g., Santos et al., 2012), which are collectively referred to as "porewater exchange" (PEX). From an ecological viewpoint, SGD is generally considered as a source of allochthonous components, whereas PEX must be viewed as a separate pathway for the autochthonous components of benthic respiration (Hong et al., 2017). In this regard, we conclude that PEX was the predominant mechanism for solute transport from the seabed into the PRE. This finding is different from our previous results in the Jiulong River Estuary, where SGD was responsible for ~50% of the total benthic input of dissolved constituents (Hong et al., 2017).

4.2. Benthic fluxes of trace metals

Based on the ratios of the concentration gradients of trace metals/^{224}Ra at the sediment–water interface, benthic fluxes of ^{224}Ra derived from ^{224}Ra/^{228}Th disequilibrium

were converted into a flux estimate of trace metals (F_i) using (Cai et al., 2014):

$$F_i = F_{Ra}\left(\frac{D_S^i}{D_S^{Ra}}\right)\left(\frac{\frac{\partial C^i}{\partial z}}{\frac{\partial C^{Ra}}{\partial z}}\right) \quad (4)$$

where $\frac{D_S^i}{D_S^{Ra}}$ is the ratio of the molecular diffusion coefficients of trace metals and ^{224}Ra in sediments, $\frac{\partial C}{\partial z}$ is the concentration gradient of trace metals and ^{224}Ra at the sediment–water interface, superscript Ra and i denote ^{224}Ra and trace metals, respectively. This method, known as the ^{224}Ra/^{228}Th disequilibrium approach, has been proved to be a reliable means of quantifying benthic fluxes of trace metals into coastal seas (Shi et al., 2018). The method is unique in that unlike the traditional core incubation method, it does not impose any interference on the natural system.

4.2.1. Barium

Benthic fluxes of Ba in the PRE varied from nil to 320 ± 99 μmol m^{-2} d^{-1} (Fig. 7 and Table 4). The highest flux was identified in the inner estuary at St. A01 with S = 3.0–7.8, and is coincident with the large Ba excess in the mixing zone that was frequently observed in the low salinity domain within the PRE (Fig. 8). This coincidence suggests that benthic input was an important source of water column Ba in the PRE.

With the benthic fluxes derived from ^{224}Ra/^{228}Th disequilibrium, we can use a multitude-box model to predict dissolved Ba concentration in the water column. This model encompasses an array of boxes within the estuary: each box receives a certain amount of seawater and river water; each box is well-mixed; each box receives an input from only the local sediments; and the boxes do not interact. We must emphasize that this is an idealized model. In a realistic estuary, an overlying water column is expected to receive inputs from a vast area of sediments along its travel path. In addition, intense horizontal mixing between two adjacent boxes can be envisioned. Despite these simplifications, the multitude-box model provides a first order estimate of dissolved Ba concentration in the water column. With this model, the net change of water column concentration of a dissolved constituent (Δi) induced by benthic input (F_i) can be estimated as:

$$\Delta i = \frac{F_i \times \tau}{H} \quad (5)$$

where H is the height of the overlying water column, and τ denotes the water residence time within the estuary. Wang (2014) has utilized a tidal prism model (Sanford et al., 1992) to derive a water residence time of 2.2 ± 0.2 d for the wet season in the PRE. Based on this estimate, changes of water column Ba concentration (ΔBa) induced by benthic input are found to range from −0.43 to 54 nmol l^{-1} ("+" denotes net increase) within the PRE (Table 4). If we adopt a riverine end-member concentration of 209 nmol Ba l^{-1}, and an open ocean end-member concentration of 40.2 nmol Ba l^{-1} (Cao et al., 2016), then dissolved Ba

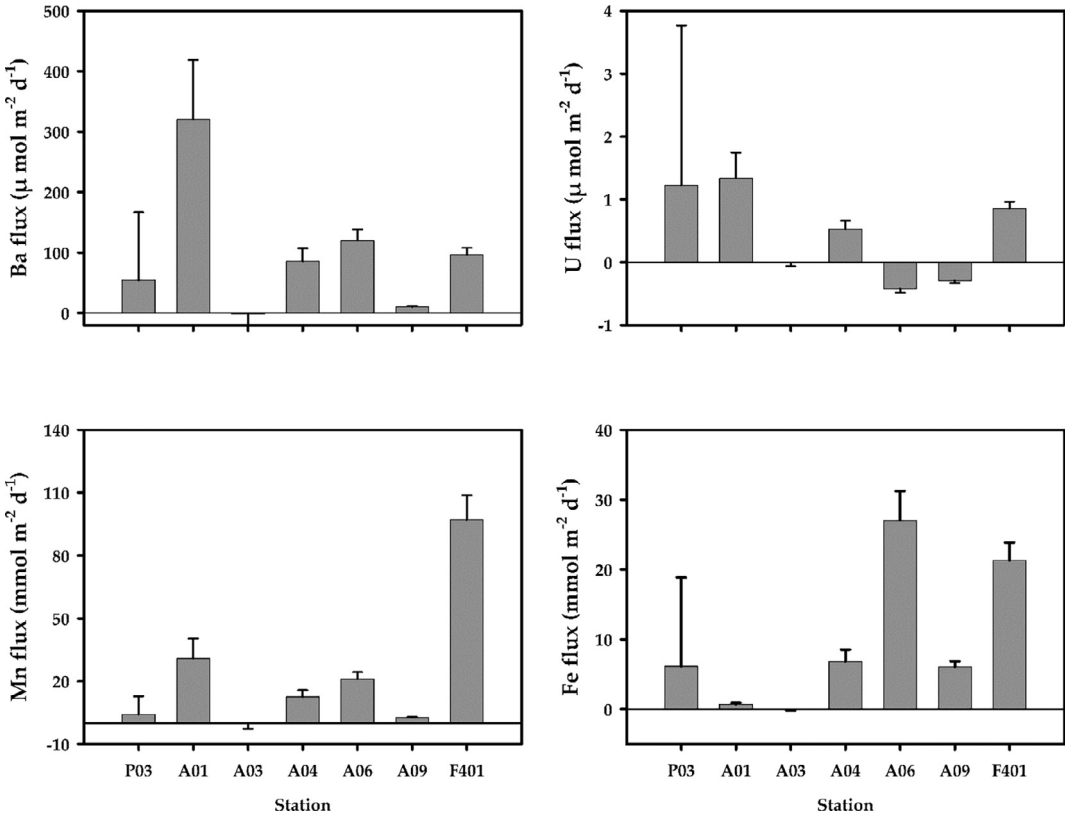

Fig. 7. Site-specific benthic fluxes of trace metals (Ba, U, Mn, and Fe) within the Pearl River Estuary.

Table 4
Concentration gradients ($\frac{\partial C_i}{\partial z}$) of dissolved trace metals (^{224}Ra, Ba, U, Mn, and Fe) at the sediment–water interface, benthic trace metal fluxes, and the net change of water column concentration (Δi) induced by porewater exchange in the Pearl River Estuary.

	$\frac{\partial C^{Ra}}{\partial z}$ dpm l^{-1} cm^{-1}	$\frac{\partial C^{Ba}}{\partial z}$ nmol l^{-1} cm^{-1}	$\frac{\partial C^{U}}{\partial z}$	$\frac{\partial C^{Mn}}{\partial z}$ μmol l^{-1} cm^{-1}	$\frac{\partial C^{Fe}}{\partial z}$	Ba flux μmol m^{-2} d^{-1}	U flux	Mn flux mmol m^{-2} d^{-1}	Fe flux	ΔBa nmol l^{-1}	ΔU	ΔMn μmol l^{-1}	ΔFe
P03	7.5 ± 1.9	796	33.2	73	108	54 ± 112	1.2 ± 2.5	4.2 ± 8.6	6.2 ± 13	13 ± 26	0.29 ± 0.59	0.98 ± 0.59	1.4 ± 3.0
A01	22.7 ± 3.5	3840	29.5	441	10	320 ± 99	1.3 ± 0.41	31 ± 9.5	0.70 ± 0.21	54 ± 17	0.23 ± 0.07	5.2 ± 0.07	0.12 ± 0.04
A03	64.9 ± 5.0	1860	11.3	290	23	−2.2 ± 18	−0.01 ± 0.06	−0.3 ± 2.4	−0.02 ± 0.19	−0.43 ± 3.5	−0.00 ± 0.01	−0.06 ± 0.01	−0.00 ± 0.04
A04	58.6 ± 4.2	2220	25.2	388	214	86 ± 21	0.53 ± 0.14	12.5 ± 3.2	6.9 ± 1.7	14 ± 3.7	0.09 ± 0.02	2.1 ± 0.02	1.2 ± 0.3
A06	26.4 ± 3.7	428	−2.8	90	115	120 ± 18	−0.42 ± 0.06	21.1 ± 3.3	27 ± 4.2	25 ± 3.8	−0.09 ± 0.01	4.4 ± 0.01	5.6 ± 0.9
A09	81.3 ± 5.8	245	−12.8	74	176	10 ± 1.4	−0.29 ± 0.04	2.6 ± 0.4	6.1 ± 0.9	0.97 ± 0.14	−0.03 ± 0.00	0.25 ± 0.00	0.59 ± 0.08
F401	44.1 ± 4.7	491	8.1	593	129	96 ± 11.7	0.86 ± 0.10	97 ± 12	21 ± 2.6	6.4 ± 0.78	0.06 ± 0.01	6.5 ± 0.01	1.4 ± 0.2

"+" denote transfer from sediments to overlying waters.

concentrations in the mixing zone of the PRE can be predicted. As shown in Fig. 8, the predicted concentration curve displays a large Ba excess in the low salinity zone. In addition, the predicted excess of dissolved Ba ($\Delta Ba = 54$ nmol l^{-1}) within this zone is in agreement with the addition of ~50 nmol Ba l^{-1} relative to the theoretical dilution line that was observed in a prior cruise. In the mid- and high salinity zone, however, the predicted concentration curve of dissolved Ba falls significantly below the observed curve. This mismatch indicates that there are extra sources of dissolved Ba in the water column, like release of Ba from suspended particles (e.g., Li and Chan, 1979).

Zeng et al. (1988) have measured Ba species in suspended particles at our sampling locations. They found that total Ba content in suspended particles decreased from a level of 1420 μg g^{-1} at the river mouth to a low of 307 μg g^{-1} near the seaward entrance. In addition, the exchangeable form and the organic form of Ba were shown to be 7.4% and 17% of the total Ba, respectively. In the present study, TSM generally decreased seaward along the estuary, from 51.3 to 8.4 mg l^{-1} (see Appendix B). If all the exchangeable fraction and a varying portion (i.e., 0–100%) of the organic fraction of Ba in suspended particles were released during estuarine mixing, then in a way similar to that described in our prior study (see Cai et al., 2015) we will estimate a total input of 0.51×10^5–1.7×10^5 mol Ba d^{-1} into the PRE. When taking the PRE as a whole, the release of Ba from suspended particles would be equivalent to an increase of 6.5–21.5 nmol Ba l^{-1} in the water column. In comparison, the total PEX fluxes would cause an input of 1.0×10^5 mol Ba d^{-1} into the PRE, or an equivalent increase of 12.8 nmol Ba l^{-1} in the water column. Taken together, the PEX input plus the release of Ba from suspended particles will lead to an increase of 19.3–34.3 nmol Ba l^{-1} in the water column. This estimate is in good agreement with prior field observation of an average addition of 26.7 nmol Ba l^{-1} relative to the theoretical dilution line in the mixing zone of the PRE (Fig. 8). However, it should be noted that the role of benthic Ba input may differ greatly in contrasting settings, depending probably on sediment lithology. As such, more measurements of ^{224}Ra/^{228}Th disequilibrium in bottom sediments will be needed to better understand the geochemical behavior of Ba in an estuary (e.g., Joung and Shiller, 2014).

4.2.2. Uranium

In contrast to Ba, sediments acted as both a source and a sink of U in the PRE. In the inner and mid-estuary, U was released from sediments at a rate of 0–1.3 μmol m^{-2} d^{-1}. In the outer estuary, it was removed into sediments at a rate of 0.29–0.42 μmol m^{-2} d^{-1}. At the seaward entrance (St. F401), sediments acted again as a source of U and released the element at a rate of 0.86 μmol m^{-2} d^{-1} (Table 4 and Fig. 7). As with Ba, we used the multitude-box model to calculate the net change of dissolved U concentration in the water column induced by the benthic input. With Eq. (5), we estimated a net change of −0.09–0.29 nmol l^{-1} for dissolved U in the water column. This is small when compared to the riverine and oceanic concentrations of dissolved U, which were determined previously to be 0.87

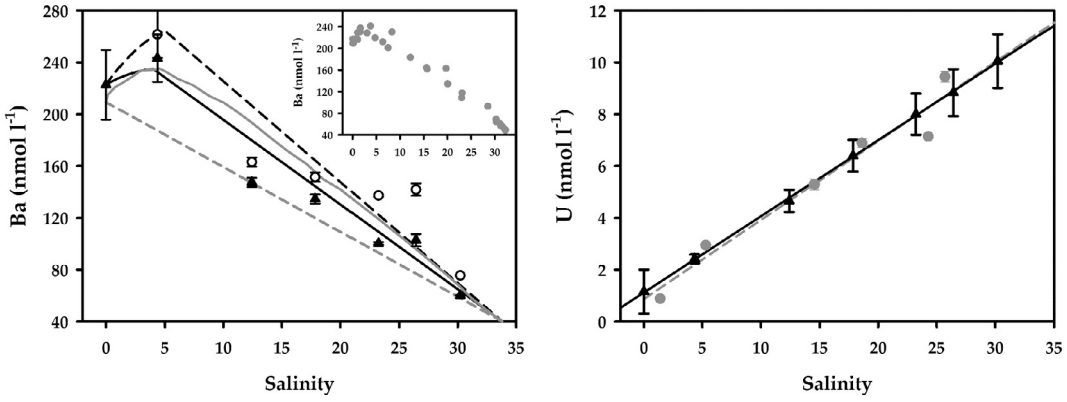

Fig. 8. Comparison of dissolved Ba and U concentrations in the water column predicted from a multitude-box model with previous field measurements within the Pearl River Estuary. The gray dash line denotes the theoretical dilution line of the riverine and coastal end-members. The end-members of Ba were taken from Cao et al. (2016), and the end-members of U were adopted from Sun et al. (1987). Field measurements of Ba in July 2012 are indicated in the box within the left graph and are shown as the gray solid line. The black line with filled triangles denotes the predicted concentrations affected only by benthic input. The black dash line with open circles denotes the upper limit of the predicted concentrations affected by both the benthic input and the release from suspended particles (i.e., all the exchangeable fraction and all the organic fraction of Ba in suspended particles were released during estuarine mixing. See the text for details).

and 14 nmol l^{-1}, respectively (Sun et al., 1987; Chen et al., 1997). As a consequence, the calculated concentration curve of dissolved U is indiscernible from the theoretical mixing line (Fig. 8). At any rate, it overlaps the observed concentration curve of dissolved U in the PRE that was derived in prior studies (e.g., Sun et al., 1987). As such, we concluded that benthic input was a minor component in the water column budget of dissolved U in the PRE.

4.2.3. Manganese and iron

Benthic fluxes of dissolved Mn and Fe estimated from $^{224}Ra/^{228}Th$ disequilibrium varied both from virtually zero to 97 mmol m^{-2} d^{-1}, and to 27 mmol m^{-2} d^{-1}, respectively (Table 4 and Fig. 7). Based on the multitude-box model, the benthic inputs would lead to an elevation of 0–6.5 μmol l^{-1} for dissolved Mn concentration, and an elevation of 0–5.6 μmol l^{-1} for dissolved Fe concentration in the water column. Prior studies, however, showed that water column concentration of dissolved Mn in the PRE was at least several times lower, and generally fell in the range of 2.0–1660 nmol l^{-1} (e.g., Wang et al., 2012). This discrepancy must be ascribed to the rapid removal of dissolved Mn and Fe during estuarine mixing (e.g., Boyle et al., 1977).

Our benthic flux estimates of dissolved Mn and Fe are also 1–2 orders of magnitude higher than historical measurements based on the traditional incubation method in other coastal seas, which range from 0 to 4450 μmol m^{-2} d^{-1}, and from <0.02 to ~2100 μmol m^{-2} d^{-1} (Pakhomova et al., 2007; Dale et al., 2015). This discrepancy might be partially caused by the temporal and spatial variability in coastal sediments. In addition, it may also be related to the inherent limitations with the incubation method (e.g., Reimers et al., 2001; Severmann et al., 2010). Nonetheless, we may evaluate the overall accuracy of our benthic flux estimates of dissolved Mn and Fe from a context of mass balance in the sediment. Let us take Fe as an example. In Chinese estuaries, highly reactive Fe (Fe_{HR}) content in sediments is 0.96–1.9 wt% (Poulton and Raiswell, 2002; Zhou et al., 2004), similar to the global average of Fe_{HR} content in coastal sediments (Raiswell and Canfield, 2012). The half-life of Fe_{HR} has been demonstrated to be <1 yr (Canfield et al., 1992). It means that on an annual basis, >50% of Fe_{HR} in sediments would be released into the overlying water column. Sedimentation rates in the PRE have been reported to vary from 1.0 to 7.0 cm yr^{-1} (Chen, 1991; Zhou et al., 2004). If we take an average sediment porosity of 0.677 and a solid density of 2.6 g cm^{-3}, then a steady-state flux of dissolved Fe can be computed:

$$\begin{aligned} F &= (1.0-7.0)\ \text{cm yr}^{-1} \times (1-0.677) \times 2.6\ \text{g cm}^{-3} \\ &\quad \times (0.96-1.9)\ \text{wt\%} \times 0.5/(56\ \text{g Fe mol}^{-1}) \\ &= 2.0-27.3\ \text{mmol Fe m}^{-2}\text{d}^{-1} \end{aligned}$$

Notably, the estimated benthic fluxes of dissolved Fe are in reasonable agreement with those derived from the $^{224}Ra/^{228}Th$ disequilibrium approach (2.0–27.3 vs. 0–27.1 mmol Fe m^{-2} d^{-1}). While the mass balance model provides only a very rough estimate of benthic dissolved Mn/Fe fluxes, agreement between independent methods lends some confidence to, or at least constrains, upper and lower limits of the overall Mn/Fe balances in the sediment. However, it is also important to emphasize that such comparisons are never ideal, because each method has its own assumptions and there are real differences in what is actually measured. In essence, two methods may agree or differ either because they are measuring different components of the local Mn/Fe pool, or are integrating over different time and space scales. For the mass balance model, it provides regional benthic flux estimates of dissolved Mn/Fe on an annual basis. In comparison, the $^{224}Ra/^{228}Th$ disequilibrium method records site-specific benthic flux events that have taken place prior to sampling, and integrates over time scales related to the mean life of ^{224}Ra ($1/\lambda = 5.3$ days). As such, short-term variability of trace metal cycles in estuarine sediments induced by high-frequency processes, like tidal movement, would be smoothed out and not be

resolved by this isotope system. Despite these limitations, it is conceivable that $^{224}Ra/^{228}Th$ disequilibrium will turn out to be a very powerful tool for quantifying benthic trace metal fluxes from coastal sediments.

5. CONCLUSIONS

Bottom sediments have long been recognized as a potential large source of trace metals in coastal seas (e.g., Jeandel et al., 2011). However, benthic fluxes of dissolved trace metals were poorly constrained and their potential impact on the water column budget was not well understood because of the limitations associated with the traditional incubation method and the complexity in coastal seas. In this study, we have extended the $^{224}Ra/^{228}Th$ disequilibrium approach to quantify benthic fluxes of trace metals (Ba, U, Mn, and Fe) into the Pearl River Estuary (PRE), China. Based on a full mass balance of ^{224}Ra in the water column, we demonstrated that porewater exchange (PEX) with scale lengths of a few centimeters was the predominant pathway for solute transport across the sediment–water interface.

With the benthic fluxes of Ba based on $^{224}Ra/^{228}Th$ disequilibrium, we demonstrated that an idealized multitude-box model can successfully reproduce the Ba excess in the water column that was frequently observed within the low salinity domain of the PRE. In comparison, the benthic fluxes of U were generally small and not expected to exert an impact on the water column budget. On the other hand, the benthic fluxes of dissolved Mn and Fe are 1–2 orders of magnitude higher than historical measurements based on the traditional incubation method in other coastal seas. Nonetheless, they are in general agreement with a simple consideration of Fe mass balance in the sediment. In this respect, this study presents a snapshot of the geochemical processes in estuarine sediments, and provides a critical addition to our understanding of the role of bottom sediments in estuarine geochemistry of Mn and Fe. This should have subsequent impact on estimates of removal fluxes due to e.g. particle scavenging in order to maintain the water column balance of these elements during estuarine mixing.

ACKNOWLEDGEMENT

This work was funded by the National Basic Research Program ("973" program) of China (Grant No. 2014CB953702), and by the National Major Scientific Research Project of China through Grant No. 2015CB954003. Support of this work also came from the Natural Science Foundation of China (NSFC) through Grants No. 41576072 and 41776083. Q. Hong appreciates the financial support for his visit to AWI through a Short-Term Research Program supported by XMU graduate school. We also thank F. Yu for providing us the TSM data, and Pingping Mi for her logistics support for the field and lab work.

APPENDIX A. POROSITY, DISSOLVED TRACE METALS (BA, U, MN, AND FE) AND ^{224}RA ($^{224}RA_D$) IN POREWATER AS WELL AS TOTAL ^{224}RA ($^{224}RA_T$) AND ^{228}TH ACTIVITIES IN THE NEAR-SURFACE SEDIMENTS OF THE PEARL RIVER ESTUARY IN JULY 2015.

Depth (cm)	Porosity (ϕ)	Ba (nmol l^{-1})	U (nmol l^{-1})	Mn (μmol l^{-1})	Fe (μmol l^{-1})	$^{224}Ra_D$ (dpm l^{-1})	$^{224}Ra_T$ (dpm g^{-1})	^{228}Th (dpm g^{-1})	$^{224}Ra/^{228}Th$ (A.R.)
Station: P03; 23.0417°N, 113.5067°E; Depth = 5.0 m; DO = 79.4 μmol kg^{-1}									
BW		217[a]	0.87[b]	[c]	*b.d.*	0.35 ± 0.02	3.25 ± 0.08	2.99 ± 0.08	1.09 ± 0.04
0–1	0.708	615	17.5	38.1	54.1	4.1 ± 0.95	4.55 ± 0.13	4.57 ± 0.13	1.00 ± 0.04
1–2	0.691	788	17.8	76.7	87.4	4.9 ± 0.85	4.56 ± 0.12	4.96 ± 0.12	0.92 ± 0.03
2–3	0.697	909	7.70	86.9	119	2.7 ± 1.2	4.82 ± 0.13	4.68 ± 0.12	1.03 ± 0.04
3–4	0.704	1040	3.63	98.9	183	5.1 ± 1.3	5.65 ± 0.16	4.27 ± 0.11	1.33 ± 0.05
4–5	0.708	1010	3.40	82.1	197	7.9 ± 2.3	5.46 ± 0.13	4.92 ± 0.11	1.11 ± 0.04
5–6	0.707	1150	3.38	78.6	238	5.8 ± 1.9	4.41 ± 0.10	4.06 ± 0.09	1.09 ± 0.04
7–8	0.700	1380	3.48	94.8	283	5.9 ± 2.8	5.91 ± 0.19	6.64 ± 0.18	0.89 ± 0.04
9–10	ND	1540	3.55	148	314	7.1 ± 1.0	5.31 ± 0.15	5.89 ± 0.14	0.90 ± 0.03
11–12	ND	2110	3.32	236	362	6.4 ± 1.1	4.90 ± 0.14	4.94 ± 0.13	0.99 ± 0.04
14–15	ND	2790	3.66	371	437	10.4 ± 1.4	4.59 ± 0.15	4.40 ± 0.13	1.04 ± 0.05
Station: A01; 22.7373°N, 113.6478°E; Depth = 13.0 m; DO = 130 μmol kg^{-1}									
BW		201[a]	1.42[b]	[c]	*b.d.*	0.54 ± 0.02	1.57 ± 0.07	2.61 ± 0.08	0.60 ± 0.03
0–1	0.740	2120	16.1	222	5.0	11.9 ± 1.7	2.07 ± 0.07	3.28 ± 0.09	0.63 ± 0.03
1–2	0.709	2510	11.7	295	38.6	19.8 ± 1.9	2.31 ± 0.07	2.78 ± 0.07	0.83 ± 0.03
2–3	0.689	3670	3.53	234	149	15.6 ± 1.8	2.47 ± 0.07	2.58 ± 0.07	0.95 ± 0.04
3–4	0.690	980	1.47	155	172	11.8 ± 2.0	1.97 ± 0.06	1.93 ± 0.06	1.02 ± 0.05
4–5	0.684	622	0.90	125	162	13.9 ± 3.0	1.92 ± 0.05	1.82 ± 0.05	1.06 ± 0.04
5–6	0.668	610	1.15	117	140	8.8 ± 2.3	1.90 ± 0.05	1.89 ± 0.05	1.01 ± 0.03
7–8	0.704	392	1.12	108	139	9.3 ± 1.4	1.94 ± 0.06	1.90 ± 0.05	1.02 ± 0.04

(*continued on next page*)

APPENDIX A. (*continued*)

Depth (cm)	Porosity (ϕ)	Ba (nmol l^{-1})	U (nmol l^{-1})	Mn (μmol l^{-1})	Fe (μmol l^{-1})	$^{224}Ra_D$ (dpm l^{-1})	$^{224}Ra_T$ (dpm g^{-1})	^{228}Th (dpm g^{-1})	$^{224}Ra/^{228}Th$ (A.R.)
9–10	0.675	403	1.39	96.1	121	11.7 ± 1.7	2.47 ± 0.07	2.43 ± 0.06	1.02 ± 0.04
11–12	0.668	612	3.33	99.7	145	13.7 ± 5.4	2.35 ± 0.07	2.28 ± 0.06	1.03 ± 0.04
14–15	ND	458	2.70	123	185	15.0 ± 3.7	2.27 ± 0.08	2.11 ± 0.07	1.08 ± 0.05
Station: A03; 22.5932°N, 113.7387°E; Depth = 11.4 m; DO = 102 μmol kg^{-1}									
BW		162[a]	5.32[b]	[c]	*b.d.*	0.56 ± 0.03	1.21 ± 0.04	2.22 ± 0.05	0.55 ± 0.02
0–1	0.750	1090	11.0	147	11.6	33.0 ± 2.5	2.80 ± 0.09	3.15 ± 0.09	0.89 ± 0.04
1–2	0.720	2124	4.21	232	147	46.9 ± 3.0	3.84 ± 0.10	4.00 ± 0.10	0.96 ± 0.04
2–3	0.708	2123	2.67	198	304	37.8 ± 3.2	3.59 ± 0.10	3.81 ± 0.10	0.94 ± 0.04
3–4	0.698	1685	3.58	168	263	32.4 ± 2.9	2.76 ± 0.09	2.47 ± 0.07	1.12 ± 0.05
4–5	0.687	1231	4.21	135	174	31.2 ± 2.5	2.70 ± 0.07	2.52 ± 0.06	1.07 ± 0.04
5–6	0.676	894	6.20	127	164	29.5 ± 2.7	2.58 ± 0.06	2.52 ± 0.06	1.03 ± 0.04
7–8	0.663	648	8.96	88.3	109	31.0 ± 2.7	3.31 ± 0.11	3.40 ± 0.10	0.97 ± 0.04
9–10	0.676	557	8.76	78.6	84.5	33.6 ± 4.1	2.70 ± 0.08	2.80 ± 0.07	0.96 ± 0.04
11–12	0.640	422	14.3	64.5	89.8	31.7 ± 3.6	2.32 ± 0.07	2.17 ± 0.06	1.07 ± 0.04
14–15	0.674	488	4.21	76.6	76.0	32.4 ± 4.5	2.26 ± 0.08	2.12 ± 0.06	1.07 ± 0.05
Station: A04; 22.5287°N, 113.7493°E; Depth = 13.0 m; DO = 110 μmol kg^{-1}.									
BW		118[a]	3.03[b]	[c]	*b.d.*	0.59 ± 0.03	0.32 ± 0.01	1.25 ± 0.02	0.26 ± 0.01
0–1	0.755	1229	15.7	196	107	29.9 ± 2.1	1.89 ± 0.06	2.29 ± 0.07	0.82 ± 0.04
1–2	0.742	1442	11.7	197	244	41.2 ± 2.4	2.76 ± 0.08	3.12 ± 0.08	0.88 ± 0.03
2–3	0.740	1513	11.1	202	305	47.7 ± 2.7	2.44 ± 0.07	2.51 ± 0.07	0.97 ± 0.04
3–4	0.702	1251	8.60	194	318	44.1 ± 2.8	2.89 ± 0.09	2.74 ± 0.08	1.06 ± 0.05
4–5	0.707	1319	8.45	192	307	50.2 ± 4.0	2.12 ± 0.05	2.06 ± 0.05	1.03 ± 0.04
5–6	0.702	828	4.09	152	278	39.6 ± 2.9	2.14 ± 0.05	2.22 ± 0.05	0.96 ± 0.03
7–8	0.678	501	7.34	119	261	38.2 ± 3.5	2.22 ± 0.08	2.60 ± 0.08	0.86 ± 0.04
9–10	0.648	475	21.5	99.9	159	44.1 ± 2.6	2.02 ± 0.06	2.39 ± 0.06	0.84 ± 0.03
11–12	0.664	487	38.1	81.2	58.8	53.8 ± 2.9	2.54 ± 0.07	2.32 ± 0.06	1.10 ± 0.04
14–15	0.629	461	55.8	63.7	47.4	49.6 ± 2.7	2.47 ± 0.08	2.35 ± 0.07	1.05 ± 0.05
Station: A06; 22.4064°N, 113.7698°E; Depth = 10.6 m; DO = 101 μmol kg^{-1}									
BW		49[a]	9.91[b]	[c]	*b.d.*	0.50 ± 0.02	0.76 ± 0.03	1.86 ± 0.05	0.41 ± 0.02
0–1	0.547	263	8.54	46.7	57.7	13.7 ± 1.8	1.31 ± 0.04	1.88 ± 0.05	0.70 ± 0.03
1–2	0.554	383	8.41	70.1	81.9	17.4 ± 1.7	1.74 ± 0.05	2.06 ± 0.05	0.84 ± 0.03
2–3	0.604	443	4.71	67.5	126	20.3 ± 2.2	1.59 ± 0.05	1.71 ± 0.05	0.93 ± 0.04
3–4	0.613	647	6.85	107	145	31.6 ± 2.9	1.64 ± 0.05	1.71 ± 0.05	0.96 ± 0.04
4–5	0.619	608	3.45	44.6	131	50.1 ± 5.2	1.61 ± 0.04	1.71 ± 0.04	0.94 ± 0.03
5–6	0.636	505	3.69	67.4	71.5	41.2 ± 3.6	1.82 ± 0.04	1.87 ± 0.04	0.97 ± 0.03
7–8	0.647	536	3.61	50.3	40.3	40.3 ± 3.0	1.66 ± 0.06	2.36 ± 0.07	0.70 ± 0.03
9–10	0.620	762	5.45	83.6	92.0	38.5 ± 2.8	1.64 ± 0.05	2.09 ± 0.05	0.79 ± 0.03
11–12	0.624	643	2.68	32.4	27.2	35.5 ± 3.0	1.73 ± 0.05	1.73 ± 0.04	1.00 ± 0.04
14–15	ND	630	1.13	24.7	30.2	38.5 ± 3.0	1.64 ± 0.06	1.78 ± 0.05	0.92 ± 0.04
Station: A09; 22.2076°N, 113.7994°E; Depth = 23.0 m; DO = 129 μmol kg^{-1}.									
BW		48[a]	9.49[b]	[c]	*b.d.*	0.52 ± 0.02	0.71 ± 0.03	1.58 ± 0.04	0.45 ± 0.02
0–1	0.711	170	3.07	38.7	87.8	41.2 ± 2.9	1.69 ± 0.06	2.40 ± 0.07	0.70 ± 0.03
1–2	0.676	176	3.18	37.8	102	43.4 ± 2.9	1.77 ± 0.05	2.15 ± 0.06	0.82 ± 0.03
2–3	0.656	196	1.99	43.1	124	42.3 ± 3.1	1.75 ± 0.05	1.84 ± 0.05	0.95 ± 0.04
3–4	0.649	218	2.07	47.0	107	51.9 ± 4.3	1.44 ± 0.05	1.53 ± 0.05	0.94 ± 0.04
4–5	0.647	184	2.91	49.2	95.5	42.1 ± 3.5	1.24 ± 0.03	1.43 ± 0.04	0.86 ± 0.03
5–6	0.640	246	2.89	55.8	92.8	37.6 ± 2.9	1.21 ± 0.03	1.34 ± 0.03	0.91 ± 0.03
7–8	0.620	213	1.88	52.4	63.4	37.1 ± 2.8	1.76 ± 0.06	1.90 ± 0.06	0.92 ± 0.04
9–10	0.615	235	1.13	48.0	60.4	37.3 ± 2.7	1.41 ± 0.05	1.42 ± 0.04	0.99 ± 0.04

(*continued on next page*)

APPENDIX A. (*continued*)

Depth (cm)	Porosity (ϕ)	Ba (nmol l^{-1})	U (nmol l^{-1})	Mn (μmol l^{-1})	Fe (μmol l^{-1})	$^{224}Ra_D$ (dpm l^{-1})	$^{224}Ra_T$ (dpm g^{-1})	^{228}Th (dpm g^{-1})	$^{224}Ra/^{228}Th$ (A.R.)
11–12	0.614	216	1.30	40.7	53.2	39.3 ± 4.1	1.15 ± 0.04	1.17 ± 0.03	0.99 ± 0.04
14–15	0.624	243	2.00	36.0	38.9	36.9 ± 3.4	1.26 ± 0.05	1.18 ± 0.03	1.07 ± 0.05
Station: F401; 22. 0839°N, 113.6448°E; Depth = 33.0 m; DO = 92.6 μmol kg^{-1}.									
BW		69[a]	6.56[b]	[c]	*b.d.*	0.40 ± 0.02	0.48 ± 0.02	1.68 ± 0.03	0.28 ± 0.01
0–1	0.770	314	10.6	298	64.5	22.4 ± 2.3	1.40 ± 0.05	2.59 ± 0.07	0.54 ± 0.03
1–2	0.735	357	9.70	299	88.8	32.1 ± 2.4	2.15 ± 0.06	2.46 ± 0.07	0.87 ± 0.04
2–3	0.730	410	6.50	293	95.0	20.0 ± 2.0	2.42 ± 0.07	2.77 ± 0.08	0.87 ± 0.04
3–4	0.716	376	7.54	296	128	41.8 ± 3.0	1.34 ± 0.05	1.82 ± 0.05	0.73 ± 0.03
4–5	0.695	355	5.93	259	138	34.1 ± 2.6	1.31 ± 0.04	1.60 ± 0.04	0.82 ± 0.03
5–6	0.669	337	4.96	219	163	16.4 ± 2.1	1.67 ± 0.04	1.80 ± 0.05	0.92 ± 0.03
7–8	0.619	389	2.62	166	132	37.9 ± 2.8	1.62 ± 0.06	2.02 ± 0.06	0.80 ± 0.04
9–10	0.673	425	1.72	144	135	41.8 ± 2.8	1.70 ± 0.05	2.23 ± 0.06	0.77 ± 0.03
11–12	0.662	487	1.26	150	154	42.1 ± 4.0	1.99 ± 0.06	2.29 ± 0.07	0.87 ± 0.04
14–15	0.593	511	0.78	134	151	38.1 ± 3.4	1.72 ± 0.06	1.84 ± 0.06	0.94 ± 0.05

BW: bottom water; $^{224}Ra_T$ and ^{228}Th in this row denote measurements in the suspended particles.
DO: dissolved oxygen in the bottom water.
: Not measured.
b.d.: Measurements indiscernible from the procedure blank of dissolved Fe (~61 nmol l^{-1}). In the calculation of the concentration gradient across the sediment–water interface, we assumed that Fe concentration in the bottom water was zero. The error caused by this assumption is small when compared to the overall uncertainty associated with the benthic flux estimates.
[a] Concentrations in BW were calculated from the relation of Ba vs. salinity based on a prior cruise in July 2012.
[b] Concentrations in BW were estimated from the linear relationship of U vs. salinity (Sun et al., 1987).
[c] Concentrations in BW were not measured here. We adopted the upper limit (1.66 μmol l^{-1}) in Wang et al. (2012) to calculate the concentration gradient across the sediment–water interface. The error caused by this treatment is small when considering the high level of dissolved Mn in porewater.

APPENDIX B. TEMPERATURE, SALINITY, TOTAL SUSPENDED MATTER (TSM), AND ^{224}RA IN THE WATER COLUMN OF THE PEARL RIVER ESTUARY

Station	Sampling depth (m)	Temperature (°C)	Salinity	TSM (mg l^{-1})	^{224}Ra (dpm 100 l^{-1})
P01	0.5	29.0	0.0	51.3	39.9 ± 2.1
P02	0.5	29.2	0.0	30.20	19.5 ± 1.3
P03	0.5	29.7	0.0	21.0	35.2 ± 1.9
A01	0.5	29.1	3.0	17.6	16.6 ± 1.2
A01	5.0	29.2	5.1	19.2	
A01	10.0	28.5	7.8	18.8	53.9 ± 2.2
A03	0.5	29.8	6.0	18.8	48.9 ± 2.5
A03	5.0	28.4	12.0	17.8	
A03	9.0	27.6	14.9	24.7	55.9 ± 2.8
A04	0.5	28.4	6.0	12.9	46.4 ± 2.2
A04	10.0	25.6	24.8	22.3	58.8 ± 2.6
A06	0.5	27.0	17.4	24.9	51.9 ± 2.6
A06	5.0	25.7	25.0	27.0	
A06	8.0	24.2	31.9	34.1	49.6 ± 2.4
A09	0.5	28.9	19.9	10.3	58.3 ± 2.4
A09	5.0	26.5	29.4	8.38	
A09	10.0	25.6	32.1	11.7	
A09	21.0	25.4	32.6	20.1	52.2 ± 2.4
F401	0.5	28.5	13.4	20.0	57.1 ± 2.8
F401	7.0	26.4	27.3	31.0	40.2 ± 2.0

REFERENCES

Berner R. A. (1980) *Early Diagenesis: A Theoretical Approach*. Princeton University Press, New Jersey.

Boyle E. A., Edmond J. M. and Sholkovitz E. R. (1977) The mechanism of iron removal in estuaries. *Geochim. Cosmochim. Acta* **41**, 1313–1324.

Cai P., Shi X., Moore W. S. and Dai M. (2012) Measurement of ^{224}Ra:^{228}Th disequilibrium in coastal sediments using a delayed coincidence counter. *Mar. Chem.* **138**, 1–6.

Cai P., Shi X., Moore W. S., Peng S., Wang G. and Dai M. (2014) ^{224}Ra:^{228}Th disequilibrium in coastal sediments: implications for solute transfer across the sediment–water interface. *Geochim. Cosmochim. Acta* **125**, 68–84.

Cai P., Shi X., Hong Q., Li Q., Liu L., Guo X. and Dai M. (2015) Using ^{224}Ra/^{228}Th disequilibrium to quantify benthic fluxes of dissolved inorganic carbon and nutrients into the Pearl River Estuary. *Geochim. Cosmochim. Acta* **170**, 188–203.

Canfield D. E., Raiswell R. and Bottrell S. H. (1992) The reactivity of sedimentary iron minerals toward sulfide. *Am. J. Sci.* **292**, 659–683.

Cao Z., Siebert C., Hathorne E. C., Dai M. and Frank M. (2016) Constraining the oceanic barium cycle with stable barium isotopes. *Earth Planet. Sci. Lett.* **434**, 1–9.

Carroll J. and Moore W. S. (1993) Uranium removal during low discharge in the Ganges-Brahmaputra mixing zone. *Geochim. Cosmochim. Acta* **57**, 4987–4995.

Chen Y. (1991) The concentration, component characteristics and the trend of deposition and dispersion of the Pearl River's sands flowing into the South China Sea. *Acta Sci. Nat. Univ. Sunyatseni* **30**, 105–112 (in Chinese with English Abstract).

Chen M., Huang Y., Chen F., Qiu Y. and Chen X. (1997) Study of dissolved uranium isotopes in some sea areas of China. *J. Oceanogr. Taiwan Strait* **16**, 285–292 (in Chinese with English Abstract).

Chow T. J. and Goldberg E. D. (1960) On the marine geochemistry of barium. *Geochim. Cosmochim. Acta* **20**, 192–198.

Cochran J. K., Carey A. E., Sholkovitz E. R. and Surprenant L. D. (1986) The geochemistry of uranium and thorium in coastal marine sediments and sediment pore waters. *Geochim. Cosmochim. Acta* **50**, 663–680.

Dale A. W., Nickelsen L., Scholz F., Hensen C., Oschlies A. and Wallmann K. (2015) A revised global estimate of dissolved iron fluxes from marine sediments. *Global Biogeochem. Cycles* **29**, 691–707.

Dymond J., Suess E. and Lyle M. (1992) Barium in deep-sea sediment: a geochemical proxy for paleoproductivity. *Paleoceanography* **7**, 163–181.

Froelich P. N., Klinkhammer G. P., Bender M. L., Luedtke N. A., Heath G. R., Cullen D., Dauphin P., Hammond D., Hartman B. and Maynard V. (1979) Early oxidation of organic matter in pelagic sediments of the eastern equatorial Atlantic: suboxic diagenesis. *Geochim. Cosmochim. Acta* **43**, 1075–1090.

Holliday L. M. and Liss P. S. (1976) The behaviour of dissolved iron, manganese and zinc in the Beaulieu Estuary, S. England. *Estuari. Coast. Mar. Sci.* **4**, 349–353.

Hong Q., Cai P., Shi X., Li Q. and Wang G. (2017) Solute transport into the Jiulong River estuary via pore water exchange and submarine groundwater discharge: new insights from ^{224}Ra/^{228}Th disequilibrium. *Geochim. Cosmochim. Acta* **198**, 338–359.

Jeandel C., Peucker-Ehrenbrink B., Jones M. T., Pearce C. R., Oelkers E. H., Godderis Y., Lacan F., Aumont O. and Arsouze T. (2011) Ocean margins: the missing term in oceanic element budgets? *EOS Trans. Am. Geophys. Union* **92**, 217–218.

Joung D. and Shiller A. M. (2014) Dissolved barium behavior in Louisiana Shelf waters affected by the Mississippi/Atchafalaya River mixing zone. *Geochim. Cosmochim. Acta* **141**, 303–313.

Joung D. and Shiller A. M. (2016) Temporal and spatial variations of dissolved and colloidal trace elements in Louisiana Shelf waters. *Mar. Chem.* **181**, 25–43.

Knox S., Turner D. R., Dickson A. G., Liddicoat M. I., Whitfield M. and Butler E. I. (1981) Statistical-analysis of estuarine profiles: application to manganese and ammonium in the Tamar Estuary. *Estuar. Coast. Shelf Sci.* **13**, 357–371.

Langmuir D. (1978) Uranium solution-mineral equilibria at low temperatures with applications to sedimentary ore deposits. *Geochim. Cosmochim. Acta* **42**, 547–569.

Li Y.-H. and Chan L.-H. (1979) Desorption of Ba and ^{226}Ra from river-borne sediments in the Hudson estuary. *Earth Planet. Sci. Lett.* **43**, 343–350.

Lovley D. R., Phillips E. J., Gorby Y. A. and Landa E. R. (1991) Microbial reduction of uranium. *Nature* **350**, 413–416.

Martin J. H. (1990) Glacial-interglacial CO_2 change: the iron hypothesis. *Paleoceanography* **5**, 1–13.

Martin J. H., Gordon R. M. and Fitzwater S. E. (1990) Iron in Antarctic waters. *Nature* **345**, 156–158.

McKee B. A., DeMaster D. J. and Nittrouer C. A. (1987) Uranium geochemistry on the Amazon shelf: evidence for uranium release from bottom sediments. *Geochim. Cosmochim. Acta* **51**, 2779–2786.

Middag R., de Baar H. J. W., Laan P., Cai P. and van Ooijen J. C. (2011) Dissolved manganese in the Atlantic sector of the Southern Ocean. *Deep Sea Res. II* **58**, 2661–2677.

Moore W. S. (1997) High fluxes of radium and barium from the mouth of the Ganges-Brahmaputra River during low river discharge suggest a large groundwater source. *Earth Planet. Sci. Lett.* **150**, 141–150.

Moore W. S. (2010) The effect of submarine groundwater discharge on the ocean. *Annu. Rev. Mar. Sci.* **2**, 59–88.

Moore W. S. and Arnold R. (1996) Measurement of ^{223}Ra and ^{224}Ra in coastal waters using a delayed coincidence counter. *J. Geophys. Res.* **101**, 1321–1329.

Murray J. W. (1975) The interaction of metal ions at the manganese dioxide-solution interface. *Geochim. Cosmochim. Acta* **39**, 505–519.

Ni H.-G., Lu F.-H., Luo X.-L., Tian H.-Y. and Zeng E. Y. (2008) Riverine inputs of total organic carbon and suspended particulate matter from the Pearl River Delta to the coastal ocean off South China. *Mar. Pollut. Bull.* **56**, 1150–1157.

Pakhomova S. V., Hall P. O. J., Kononets M. Y., Rozanov A. G., Tengberg A. and Vershinin A. V. (2007) Fluxes of iron and manganese across the sediment–water interface under various redox conditions. *Mar. Chem.* **107**, 319–331.

Poulton S. W. and Raiswell R. (2002) The low-temperature geochemical cycle of iron: from continental fluxes to marine sediment deposition. *Am. J. Sci.* **302**, 774–805.

Raiswell R. and Canfield D. E. (2012) The iron biogeochemical cycle past and present. *Geochem. Perspect.* **1**, 1–220.

Reimers C. E., Jahnke R. A. and Thomsen L. (2001) In-situ sampling in the benthic boundary layer. In *The Benthic Boundary Layer: Transport Processes and Biogeochemistry* (eds. B. P. Boudreau and B. B. Jorgensen). Oxford University Press, Oxford, pp. 245–268.

Sanford L. P., Boicourt W. C. and Rives S. R. (1992) Model for estimating tidal flushing of small embayments. *J. Waterw. Port Coast. Ocean Eng.* **118**, 635–654.

Santos I. R., Eyre B. D. and Huettel M. (2012) The driving forces of porewater and groundwater flow in permeable coastal sediments: a review. *Estuar. Coast. Shelf Sci.* **98**, 1–15.

Scholz F., McManus J., Mix A. C., Hensen C. and Schneider R. R. (2014) The impact of ocean deoxygenation on iron release from continental margin sediments. *Nat. Geosci.* **7**, 433–437.

Severmann S., McManus J., Berelson W. M. and Hammond D. E. (2010) The continental shelf benthic iron flux and its isotope composition. *Geochim. Cosmochim. Acta* **74**, 3984–4004.

Shi X., Mason R. P., Charette M. A., Mazrui N. M. and Cai P. (2018) Mercury flux from salt marsh sediments: insights from a comparison between $^{224}Ra/^{228}Th$ disequilibrium and core incubation methods. *Geochim. Cosmochim. Acta* **222**, 569–583.

Sun H., Liu S., Zhang H., Wu L. and Zhang C. (1987) A preliminary study on uranium distribution and its isotopic composition in Zhujiang estuarine water. *Trop. Oceanol.* **6**, 55–60 (in Chinese with English Abstract).

Wang S. (2014) *Submarine groundwater discharge and associated fluxes of nutrients and carbon into the Pearl River estuary*. Xiamen Univ, Master (in Chinese with English Abstract).

Wang D., Lin W., Yang X., Zhai W., Dai M. and Arthur Chen C.-T. (2012) Occurrences of dissolved trace metals (Cu, Cd, and Mn) in the Pearl River Estuary (China), a large river-groundwater-estuary system. *Cont. Shelf Res.* **50–51**, 54–63.

Zeng X., Zheng J., Lin Z., Liang Z. and Chan K. (1988) Interfacial geochemistry of barium in suspension and sediment from Zhujiang Estuary. *Acta Oceanol. Sin.* **9**, 247–254 (in Chinese with English Abstract).

Zhang J. (2014) The variation of biodiversity of macrobenthic fauna with salinity and water depth near the Pearl Estuary of the northern South China Sea. *Biodivers. Sci.* **22**, 302–310 (in Chinese with English Abstract).

Zhao H. (1990) *Evolution of the Pearl River Estuary*. China Ocean Press, Beijing (in Chinese).

Zhou H., Peng X. and Pan J. (2004) Distribution, source and enrichment of some chemical elements in sediments of the Pearl River Estuary, China. *Cont. Shelf Res.* **24**, 1857–1875.

Associate editor: Anthony Dosseto